RSC Advances

ROYAL SOCIETY OF CHEMISTRY

www.rsc.org/advances

RSC Advances

RSCPublishing

ARTICLE

A template-free facile approach for the synthesis of CuS/rGO nanocomposites towards enhanced photocatalytic reduction of organic contaminants and textile effluents

Cite this: DOI: 10.1039/x0xx00000x

Received 00th January 2012,
Accepted 00th January 2012

DOI: 10.1039/x0xx00000x

www.rsc.org/

Murugan Saranya,[a] Rajendran Ramachandran,[a] Pratap Kollu,[b] Soon Kwan Jeong[c*] and Andrews Nirmala Grace[a,c,*]

Copper sulfide/reduced graphene oxide nanocomposites were synthesized hydrothermally from copper nitrate and thiourea as precursor materials. In the hydrothermal route, rGO is formed by the reduction of GO with simultaneous formation of CuS/rGO nanocomposites. The CuS/rGO nanocomposites was investigated using powder XRD, FE-SEM, HR-TEM, DRS UV-vis spectroscopy, photoluminescence (PL) measurements, infra-red spectroscopy and photoelectron spectroscopy (XPS). DRS UV-vis measurements of CuS/rGO nanocomposites feature a strong absorption in the range 400–800 nm, which suggests that they have photocatalysis applications. Three different composites were prepared with different loadings of rGO to study the effect of loading on methylene blue (MB) dye degradation. The photocatalytic properties of the composites were tested in a visible light photoreactor chamber. The CuS/rGO nanocomposites were found to exhibit high photocatalytic activities with a maximum efficiency of 99.27% after 60 min in visible source. These interesting and enhanced catalytic properties of CuS/rGO-x nanocomposite was further tested for the organic contaminant and textile effluents collected from two different sites situated in the Thirupur textile industries, India. Results showed the CuS/rGO-x nanocomposite is an efficient photocatalyst.

Introduction

Dyes and pigments are major organic pollutants because they are often toxic and non-biodegradable. A recent development in photocatalysis is the advanced oxidation process (AOP), which is considered an effective technology for dye degradation that can be used instead of conventional methods.[1,2] The main focus has been the development of visible light photocatalysts because visible light accounts for approximately 42% of solar radiation energy, whereas UV light (ultra violet) provides only 3-4%. Although TiO_2 is currently considered as the most important semiconductor photocatalyst due to its non-toxicity and high thermal stability, its photocatalytic properties are limited by its rapid charge-carrier recombination.[3] The photocatalytic properties of many other semiconductors, such as sulfides and metal oxides ZnS, ZnO, CdS, PbS, and WO_3, have been investigated.[4] The wide band gaps of these materials mean that their photocatalysis processes require UV irradiation. In contrast, chalcogenides act as photocatalysts in visible light. Among the various semiconducting materials, copper based catalysts have gained more attention because of its distinguished catalytic properties in wide range of water treatment applications. CuS is a metal chalcogenide and an important p-type semiconducting material existing in a vast range of stoichiometric forms.[5] Depending upon their Cu to S stoichiometric ratios, these copper sulfides behave as direct band or indirect band gap semiconductors. CuS-based catalysts have shown promise as highly efficient, low cost materials for the processing of environmental contaminants. Copper sulfides have an enormous range of applications and unique chemical, physical, optical and electronic properties.[6]

In particular, copper sulfide (CuS) can be prepared with morphologies such as nanoflowers, nanoplates, nanotubes, nanorods, nanoflakes, nanospheres, nanocubes and complex hierarchical micro/nanostructures.[7-11] The unique morphology of these nanostructures is based on nanoscale aggregation and the nanoparticle units comprise the secondary structures, which

are expected to improve and promote the photocatalytic properties of these materials. A new focus of research in this area is the growth of hierarchical structures for use in catalytic processes.[12] Fascinating CuS structures with good crystallinity have successfully been used in visible light dye degradation.[13,14]

During the past decade, numerous attempts have been made to improve semiconductor photocatalyst performance through doping with non-metals like boron and fluorine,[15] noble metal loading,[16] and the preparation of semiconductor composites.[17] Graphene-based materials have received much attention. Graphene is a 2D-graphitic carbon system with very high surface area (~2600 m^2/g) and superior electron mobility and thermal and electrical conductivity as well as excellent physical, optical, mechanical, electrical, and thermal properties.[18,19] Graphene is a promising material in various niche areas of nanoscience, with applications in electrochemical devices,[20] catalysis and energy storage,[21,22] ascorbic acid adsorption and biosensors[23,24] and medical applications.[25] The introduction of graphene and graphene oxide (GO) into semiconductors can alter their physical and chemical properties. There have been a number of reports on the preparation of hybrid nanostructures of metal oxide based composites with graphene sheets, but not much attention has been paid to chalcogenide-based nanocomposites for photocatalytic applications.[26] These preparation methods include electrophoretic deposition,[27] co-precipitation,[28] microwave assisted,[29] chemical,[30] electrochemical synthesis,[31] sol-gel,[32] UV-assisted photocatalytic synthesis[33] and solvothermal and hydrothermal.[34-36]

The hydrothermal method is the most appealing method because it could be operable at less temperature with high efficiency and could be scaled up. The use of surfactant and template may increase the complexity of the reaction process, which results in im purity of the products. It is thus necessary to develop a facile, surfactant and template free method for the CuS synthesis. This pioneering work has stimulated extensive research into the preparation and applications of GO-based CuS nanostructures with surfactant and template-free methods. CuS is as a narrow band gap semiconductor, which requires only visible light for photocatalytic activity and rGO exhibits high visible light activity in dye degradation. Also, rGO can modulate the electronic structure of metal and semiconductor nanoparticles. The rGO can induce easier electron transfer from the conduction band of semiconductor (CuS) or the excited dye to rGO due to the large energy level offset formed at the interface leading to enhancement in photocatalytic activity. In this study, CuS/rGO nanocomposites with various rGO loadings and diverse morphological structures denoted as CuS/rGO-x,y,z were prepared via a simple hydrothermal route. The photocatalytic properties of these CuS/rGO nanocomposites with respect to methylene blue dye degradation were investigated. One of the CuS/rGO nanocomposites with a particular rGO loading was found to exhibit good photocatalytic degradation of MB dye with an efficiency of 99.27%. The kinetics of the photodegradation and the recyclability of the nanocomposites are also discussed. To further know the practical utility of the photocatalyst, the samples contaminated with multi dyes were collected from textile industries near Thirupur, Tamil Nadu, India and tested with our prepared catalyst.

Experimental

Materials

Graphite powder, hydrogen peroxide (30 wt %), sodium nitrate (98%), sulfuric acid (98 wt %), potassium permanganate, hydrazine hydrate (98%), ammonia (30%), copper nitrate trihydrate (99%), thiourea (98%), methylene blue and 4-nitrophenol from SD Fine chemicals, India were used.

Synthesis of graphene oxide

Hummers route was adopted for the preparation of GO.[37] To graphite (known amount), concentrated sulphuric acid was mixed and stirred continuously for 24 h. 100 mg of sodium nitrate and 3 g of potassium permanganate were then added under ice-cold conditions. After stirring, the temperature was raised to 35-40°C and to it DI water was added and further the reaction was maintained at 98°C. The reaction was stopped by the addition of distilled water and hydrogen peroxide to obtain a bright yellow suspension. The same was centrifuged with 5% HCl, ethanol and kept in an open atmosphere and dried. The prepared GO was then ultrasonicated in DI water to obtain individual sheets.

Synthesis of CuS/rGO nanocomposites

The CuS/rGO nanocomposites were prepared with the hydrothermal method. To 40 mL of DI water, 1 mmol of copper nitrate was added and the solution was stirred continuously. When a blue solution had formed, 2.5 mmol of thiourea was immediately added. Once the solution was well dispersed, 20 mg of rGO was added to the mixture and autoclaved at 150°C for 24 hours. The black precipitate was centrifuged with distilled water, ethanol and kept at RT to produce CuS/rGO-x nanocomposite.[38] The above procedure was repeated for 40 mg and 60 mg graphene to produce the CuS/rGO-y and CuS/rGO-z nanocomposites respectively. For comparison, bare CuS was synthesized with a similar method in the absence of rGO.

Characterization

CuS/rGO composites were investigated by performing XRD (Philips X'Pert PRO) with a radiating wavelength of 0.154 nm. Surface morphologies were analyzed with high-resolution TEM by using a JEOL-2000EX operated at 120 kV and FE-SEM, model-Hitachi SU6600. The optical and photocatalytic phenomena of CuS nanostructures were probed with Hitachi U-2800 spectrophotometer. The photoluminescence properties were determined with a fluorescence spectrometer (Horiba Jobin Yvon - Fluorolog) and the functional groups were

analyzed by performing FT-IR spectroscopy (Shimadzu Affinity-1). Photoelectron spectroscopic measurements were done by a Thermo Scientific Multilab spectrometer. The XPS spectra were normalized with reference to 284.6 eV, pertaining to C1s, and the graphs were analyzed with Casa software.

Photoreactor set-up

For photocatalysis experiment, a home-made reactor was set-up with a photo chamber and water cooling system, as given in Scheme 1.

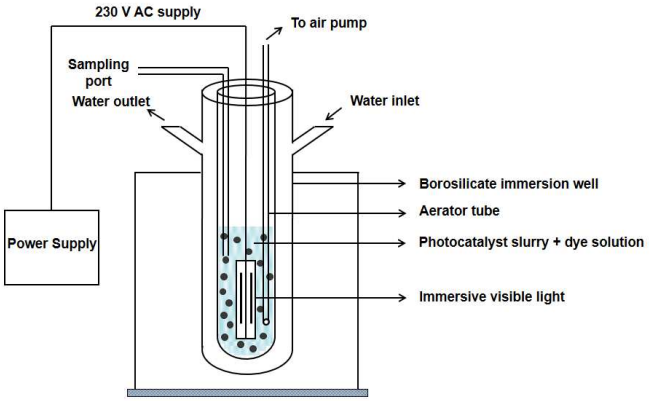

Scheme 1 Schematic representation of reactor set-up used in the photocatalytic experiment

For photocatalysis experiment, a home-made reactor was set-up with a photo chamber and water cooling system, as given in Scheme 1. The reactor has a borosilicate immersion well with a water inlet and a water outlet. A 150 W visible tungsten light source supplied with an AC power of 230 V was used and kept immersed in the MB dye solution. The dye slurry and the photocatalyst were continuously stirred by using an aerator tube connected to the well. A sampling port is present in the chamber for periodical sampling.

Photodegradation experiment

The CuS/rGO nanocomposites were tested as photocatalysts by monitoring the photodegradation of aqueous solutions of methylene blue (MB) dye. Visible light was used as source for the photodegradation studies. In brief, for the investigation, dye slurry is made by the following protocol: added 30% of 2 mL of HP into 50 mL of 20 mg/L methylene blue suspension with 30 mg CuS/rGO photocatalyst. For all the experiments using different photocatalyst, equal amount of catalyst was taken. To attain an adsorption/desorption equilibrium state, the dye slurry were mixed in dark for 30 min. The suspension was sampled at certain time intervals; approximately 1 mL of solution was extracted, diluted, and centrifuged for 10 min to discard the catalyst. The dye concentrations were observed with ultraviolet spectrometer by measuring the methylene blue absorption at 663 nm. To compare with the CuS/rGO catalyst, commercial TiO_2, rGO, and CuS without rGO were also tested. Also the degradation properties were tested for the organic contaminant and the textile industries effluents under similar conditions. The collected effluent samples were used as such without any prior treatment.

Results and discussion

Structural and morphological analysis

The phase compositions and crystal structures of the CuS/rGO nanocomposites were studied with XRD, the resulting patterns are given in Fig. 1. In these patterns, a diffraction peak is evident at 10.6°, which corresponds to the graphene plane (002). These characteristic (002) peaks of graphene are not intense, revealing the formation of non-stacked sheets of graphene during its synthesis. Further, CuS growth on graphene sheets prevents the stacking process.[39] The absence of graphene oxide peak in the XRD patterns shows the effective reduction of GO to rGO. Diffraction peaks were observed at 27.6 (101), 29.6 (102), 31.7 (103), 32.8 (006), 47.9 (110), 52.7 (108) and 59.3 (118) suggesting the formation of pure CuS as in accordance with JCPDS card no. 06-0464 with cell parameters a:3.792 Å and c:16.344 Å. Thus the prepared final products are highly crystalline and consist of pure hexagonal phase.

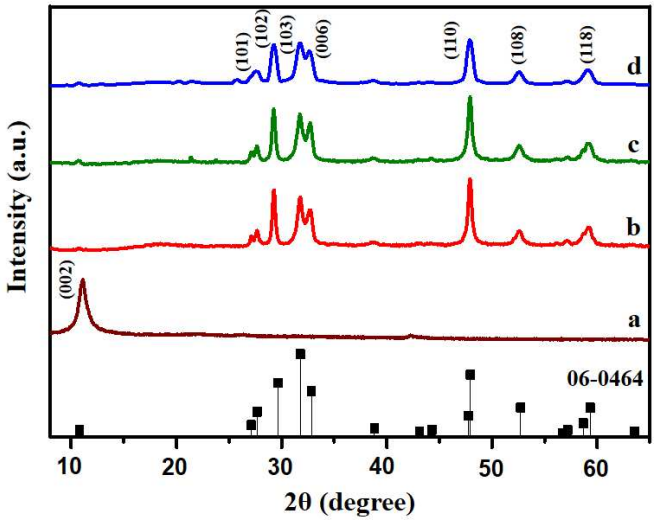

Fig. 1 X-ray diffraction patterns of (a) pure GO, (b) CuS/rGO-x (c) CuS/rGO-y and (d) CuS/rGO-z nanocomposites

No other peaks other than those characteristic of CuS could be seen. The crystallinity of CuS is retained in the nanocomposites, as demonstrated by the XRD patterns, which indicate that the addition of GO does not change the crystal orientations of the CuS nanocomposites.

The FE-SEM images of the CuS/rGO nanocomposites with various rGO ratios are shown in Fig. 2. These images indicate the presence of numerous nanoplates of self-assembled cylindrical flower-like CuS structures, which are formed due to van der Waals forces. The energy dispersive X-ray results from the SEM images clearly confirms the increase in the carbon content of the CuS nanostructures with increase in the graphene

loading (Fig. 3). Fig. S1 shows the HR-TEM images of CuS/rGO nanocomposites. The low magnification HR-SEM images is given in Fig. S2, which shows distribution of CuS on rGO.

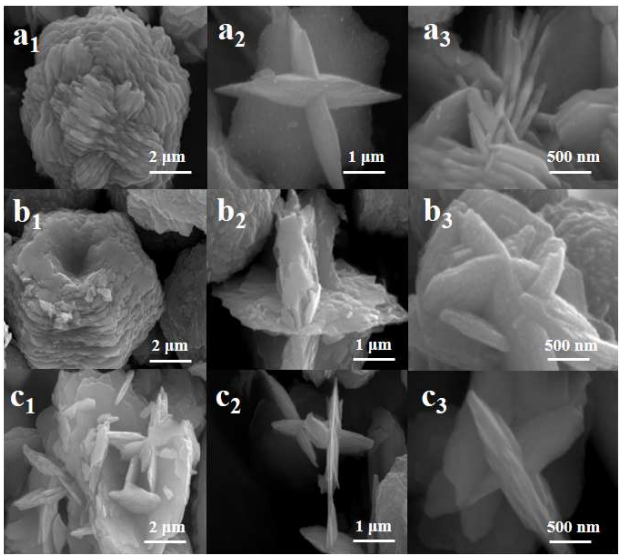

Fig. 2 Field emission SEM images of CuS/rGO nanocomposites (a) CuS/rGO-x (b) CuS/rGO-y and (c) CuS/rGO-z at different magnifications

We then investigated the mechanism of the formation of the CuS nanostructures. It is well known that the formation of copper nitrate/thiourea complexes occurs during the hydrothermal growth of CuS nanostructures. The formation of the CuS nanostructures occurs in three steps: in the initial stage, thiourea reacts with Cu^{2+} to form copper-thiourea complexes giving CuS primary nanoparticles during the hydrothermal treatment. Here temperature plays a vital role: at lower temperatures, thin flakes or platelets of CuS nanostructures are formed in the initial stage with less aggregation.

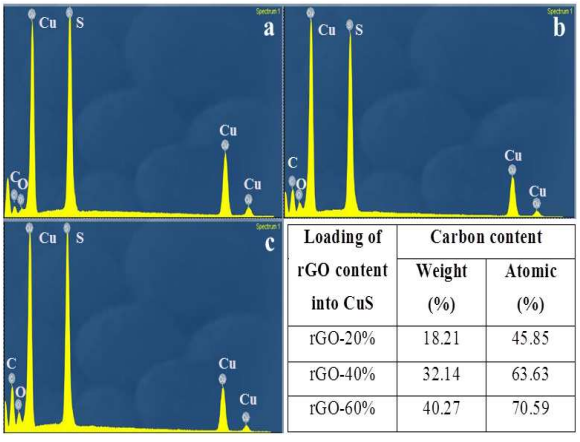

Loading of rGO content into CuS	Carbon content	
	Weight (%)	Atomic (%)
rGO-20%	18.21	45.85
rGO-40%	32.14	63.63
rGO-60%	40.27	70.59

Fig. 3 EDX spectra of CuS/rGO nanocomposites (a) CuS/rGO-x (b) CuS/rGO-y (c) CuS/rGO-z and different loading % of rGO with CuS

Nucleation occurs via the Ostwald ripening process.[40] In the second step, these primary particles aggregate and the CuS nuclei grow preferentially in the same direction to become CuS nanoplates. The aggregation of the nanoparticles is due to primary atomic forces like van der Waals, π-π interactions.[41] Finally, these nanoplatelets interact with each other, which results in the formation of self-assembled CuS composites with larger diverse flower-like architectures, given in Fig. 2. A high temperature promotes the formation of homogeneous CuS nanostructures. The growth phase and the nucleation phase are controlled to produce well-defined morphologies.

Optical Properties

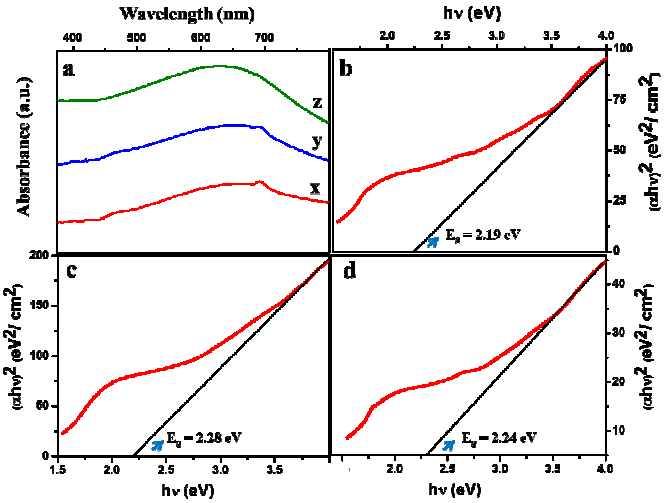

Fig. 4 (a) Diffusive reflectance UV-Vis Spectra of CuS/rGO nanocomposites (x,y,z represents loading ratio of rGO) and corresponding band gap spectra of rGO nanocomposites (b) CuS/rGO-x (c) CuS/rGO-y and (c) CuS/rGO-z

The UV-vis diffusive absorption spectrum of CuS/rGO is shown in Fig. 4a. There is a strong absorption in the spectra of the CuS composite samples in the region 400 to 800 nm.[42] The absorption spectra of the three samples are almost identical; each contains a shoulder around 650 nm. These results indicate that CuS is a promising material in the photocatalytic field. The optical band gap was calculated in accordance with Eq. (1). To calculate the band gap energy, $(\alpha h\upsilon)^2$ vs. $(\alpha\upsilon)$ was plotted, where α and $h\upsilon$ are the absorption coefficient and energy of photons respectively, A-constant, with n either 2 for direct transitions or 0.5 for indirect transitions and E_g is the band gap.[43]

$$(\alpha h\upsilon)^n = A(h\upsilon - Eg) \quad (1)$$

According to Eq. (1), which is based on direct transitions, the band gaps of the as-obtained CuS nanocomposites are 2.19, 2.28, and 2.24 eV, as shown in Fig. 4b-d. The band gap values do not vary remarkably with increase in the graphene loading. These band gaps are higher than the bulk value, which could be due to quantum confinement in the small crystalline CuS nanostructures.[44] Fig. 5a shows the PL spectra of the CuS/rGO

nanocomposites at room temperature. Excitation at 400 nm results in a broad emission peak at 499 nm (2.48 eV). It has been concluded that the emission spectra of CuS samples mainly depend on their morphologies and inherent structures.[45] The peak position is the same in all three cases, although the intensity does vary, which could be related to CuS size effects.[46,47]

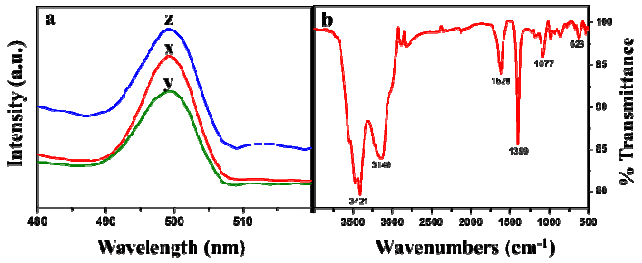

Fig. 5 (a) PL spectra of CuS/rGO nanocomposites (a) CuS/rGO-x (b) CuS/rGO-y and (c) CuS/rGO-z and (b) FT-IR spectra of CuS/rGO-x nanocomposites

The IR spectrum of CuS/rGO nanocomposites is given in Fig. 5b. Strong absorption peaks around 3421 cm^{-1} and 3149 cm^{-1} are due to the hydroxyl group stretching nodes and the peak at 1620 is attributed to the bending vibrations mode of O-H groups of absorbed water. The vibration mode absorbs at 1399 cm^{-1} and that of C-O stretching at 1077 cm^{-1}. CuS stretching mode adsorbed at 628 cm^{-1}.[48]

XPS analysis

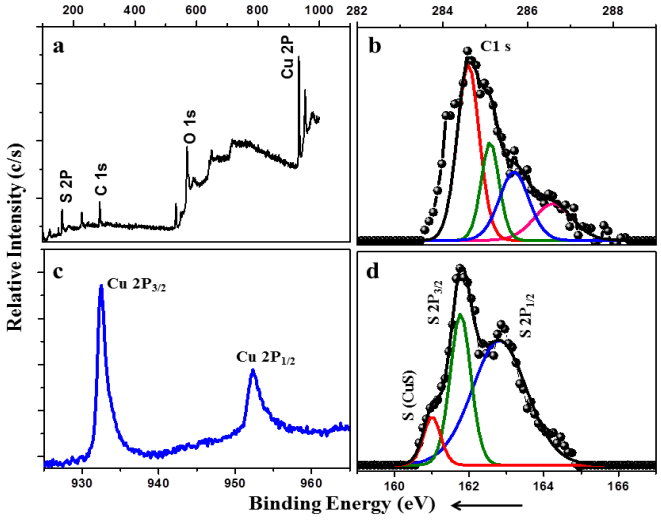

Fig. 6 (a) Wide scan XPS survey and high resolution deconvoluted XPS spectrum (b) C1 s, (c) Cu 2p and (d) S 2p of CuS/rGO-x nanocomposites

To further explore the surface electronic state and elemental composition of the composite, XPS were recorded and the results manipulated keeping C1s peak as reference (Fig. 6). From the wide scan survey, 2p (Cu), 2p (S), 1s (O) and 1s (C) peaks were observed. The deconvoluted C1 s peak is given in Fig. 6b and could be observed are three Gaussian peaks centered at 284.6, 285.6 and 286.1 eV. The C-C bond of sp2 carbon atom in reduced GO could be assigned to 284.6 eV and the other peaks (285.0 eV, 286.1 eV) is due to C=C and C-O (epoxy and hydroxyl) respectively.[49] Fig. 6(c), shows the deconvoluted spectrum of Cu 2p peak and as seen from the analysis, the binding energies at 932.5 eV correspond to 2p3/2 (Cu) and the one at 952.3 eV is due to 2p1/2 (Cu). Also a shakeup satellite peak are observed around 943 eV, characteristic of Cu(II) which indicates the paramagnetic Cu^{2+} state.[50] In the case of S 2p region, a doublet peak at 162.0 eV could be seen characteristic for metal sulfides, which is associated with 2p3/2 (S) and 2p1/2 (S) and an additional small peak at 161.0 eV attributed to CuS.[51]

Visible light photocatalytic activity

The catalytic activities for the prepared CuS/rGO catalyst with respect to decomposition of MB were investigated. The visible light photocatalytic efficacy of CuS-rGO samples were evaluated by monitoring the MB decolorization rates.

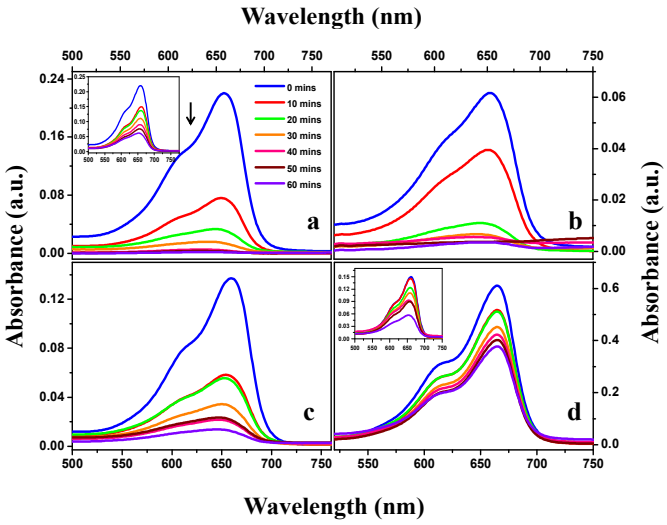

Fig. 7 Phodegradation of MB dye in visible light irradiation using (a) CuS/rGO-x (inset figure – CuS with 10% loading of rGO) (b) CuS/rGO-y (c) CuS/rGO-z and (d) Degussa P25 TiO2 (inset figure - pure CuS without rGO)

A decrease in the intensity of the 663 nm absorption peak was followed and evaluated to study the degradation of the dye. Fig. 7 shows the drift in the absorption spectrum of methylene blue under visible light over different time intervals. These results show the effects of varying the graphene loading in the nanocomposites. As the irradiation time increases, the peak at 663 nm declines in intensity indicating the degradation of MB. Upon further light exposure, the absorption peak intensity drops rapidly with time (Fig. 7) and has almost vanished completely after 60 min. According to this figure, the CuS/rGO-x nanocomposite, which has an rGO loading of 20%, exhibits the highest photocatalytic activity. After irradiation with visible light for 60 min, the degradation fractions for the photocatalysts

are 99.27% for CuS/rGO-x, and 94% and 89% for CuS/rGO-y and CuS/rGO-z respectively. The photocatalytic activity has been tested for 10% rGO loading with CuS, but results showed only negligible degradation of MB dye (inset of figure 7 (a)). Results showed that the presence of graphene has improved the efficiency but got saturated at a particular loading of graphene viz. 20%. This could be because of the stacking effect of graphene at higher loadings.[52] The low GO loading helped to prevent CuS from severe aggregation, which is beneficial for the distribution of CuS nanoparticles over GO planes. High GO loading beyond 10% loading led to the aggregation of CuS nanoparticles and undesirable staking of GO sheets.[53] The higher reduction degree of GO at low GO loading promotes the transfer of electrons CuS and GO, which is beneficial for the degradation of methylene blue. Thus CuS/rGO-x exhibits excellent photocatalytic activity in the visible region and rGO contributes equally towards the degradation of the dye.

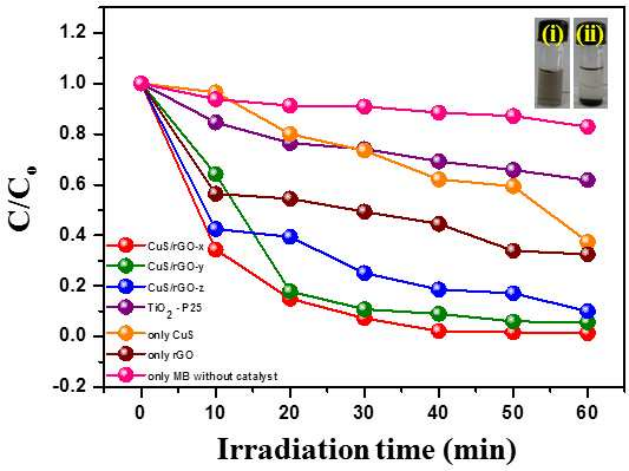

Fig. 8 Variation of MB concentration after the absorption equilibrium at different time intervals in the presence of CuS/rGO-x photocatalysts (inset shows (i) before and (ii) after 10 min of sedimentation of 1 h photocatalysed CuS/rGO-x nanocomposite)

For comparison, we assessed the activity of the commercially available Degussa P25 TiO_2 nanopowder and pure CuS (see the inset in Fig. 7d) without rGO. The CuS/rGO photocatalysts exhibited and enhanced effect than P25 TiO_2 powder and pure CuS catalyst. To know the effect of the composites, the photocatalytic activity of a mixture of CuS and rGO, mixed by physical stirring was measured and the results show only 71.43% degradation, which was less when compared to CuS/rGO composites which is given Fig. S3. These results show that the effect is not merely due to the individual elements but due to the composite formation and the synergistic effect between them. This enhanced photocatalytic activity could be attributed to the synergistic effect that arises between the rGO and CuS nanoparticles, which significantly reduces charge recombination. In addition to this, the CuS/rGO nanocomposite materials exhibited good sustainability, as evidenced by their consistent photocatalytic performance and the absence of any observable changes in morphology, even after five cycles of operation during photocatalytic experiments (Fig. 10). The overall results of the study indicate that these newly prepared photocatalytically stable CuS/rGO nanocomposites could be potentially utilized for many environmental remediation applications. Pure rGO was also tested and found to exhibit negligible activity.[54]

In accordance with the Beer-Lambert's theory, the dependence of methylene blue concentration to the absorption peak intensity at 663 nm is linear. Hence the following equation was adopted to calculate the decomposition efficacy of MB dye:

$$Degradation\ Rate(\%) = (1 - \frac{A_t}{A_o}) \times 100 \quad (2)$$

where A_t and A_o are the absorbance at reaction time t and initially.

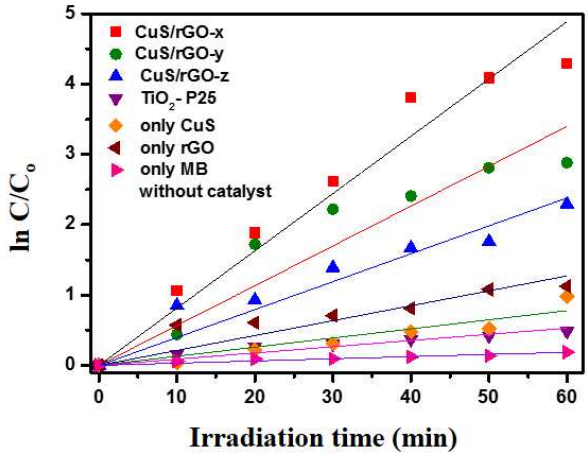

Fig. 9 Kinetic fit plot of ln (C/Co) vs time for different photocatalyst under visible light irradiation

The corresponding C/C_o graph is given in Fig. 8 and compared with those for the Degussa TiO_2 catalyst, CuS without rGO, and rGO; the CuS/rGO samples exhibit enhanced photocatalytic efficiencies. CuS/rGO-x exhibits the highest photocatalytic activity of 99.27% over a period of 1 hr. Fig. 8 gives the variation of concentration of residual MB with irradiation time. All three photocatalysts produce drastic decreases in the dye concentration; the maximum decrease is that due to the CuS/rGO-x catalyst.

Eco-friendly photomaterials should be easily separated and removed from the experimental set-up. Sedimentation analyses were run for the samples photodegraded in the presence of the CuS/rGO-x catalyst, as shown in the inset in Fig. 8. This figure clearly shows that the particles sediment completely in 10 min, which indicates that the catalyst can easily be recovered. The corresponding kinetic fit plot of $\ln(C/C_0)$ vs. time obtained from the results in Fig. 8 is shown in Fig. 9.

Stability and reusability are further vital considerations for the assessment of the nanocomposites because photoanodic corrosion will limit their stability. The photocatalytic stabilities of the nanocomposites were assessed by recycling them from

their aqueous systems and reusing them in repeated MB degradation experiments (Fig. 10). This figure shows that up to 99.27% (almost 100%) of MB is degraded after 60 min in the first cycle of degradation and from the second to fifth cycle, 97.8%, 96.3%, 95.2%, and 93.3% of MB degradation could be observed. Thus the efficiencies with respect to the photodegradation of MB dye of the pristine catalyst and the photocatalyst reused in five cycles are nearly the same. The recyclability test was done for all the other photocatalyst but results showed that the degradation drastically decreased over cycles as compared to the CuS/rGO-x catalyst. Thus the CuS/rGO photocatalyst is stable with respect to MB dye degradation.

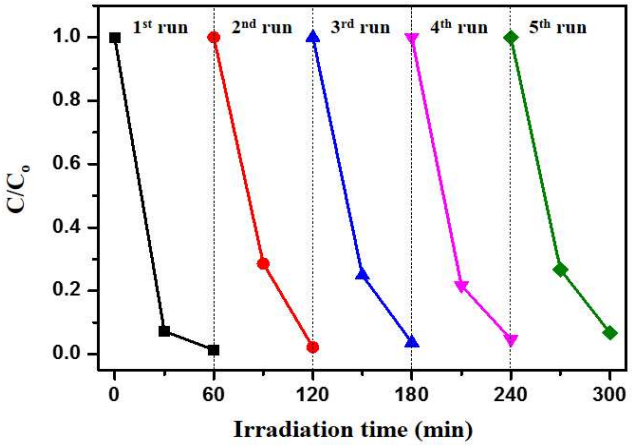

Fig. 10 The repeated degradation cycle of CuS/rGO-x nanocomposites in MB solution under visible light irradiation

Table. 1 Comparison of catalytic activity of various graphene nanocomposites towards methylene blue dye degradation

Material[a]	DC[b]	CD[c]	LS[d]	IT[e]	D[f]	R[g]
Graphene@ TiO_2	10	0.5	UV	<100	88	[56]
P25–graphene	10	0.4	UV	200	>90	[57]
Graphene–Cu_2O	10	0.4	Visible	120	90	[58]
La/TiO_2-graphene	10	1	Visible	60	>80	[59]
TiO_2–GO	10	0.5	Visible	180	>80	[60]
rGO/TiO_2	20	0.2	UV	45	>80	[61]
ZnO/rGO	10	0.5	UV	180	>90	[62]
rGO/ Ta_2O_5	10	0.5	UV	120	79	[63]
Ag_3PO_4/ rGO	10	0.28	Visible	90	72	[64]
CuS/rGO	4	0.1	Visible	120	>81	[65]
rGO–CdS	100	0.16	Visible	150	94	[66]
CuS/rGO-x	20	0.6	Visible	60	>99	This work

[a] Photoactive Nanocomposite. [b] Initial dye concentration (mg L^{-1}). [c] Catalyst dosage (g L^{-1}). [d] Light Source. [e] Irradiation time (mins). [f] Degradation (%). [g] Reference.

The small decrease in photocatalytic activity that results from this reuse could be due to unavoidable photocatalyst loss during centrifugation and the accumulation of organic compound intermediates, which might indirectly affect dye adsorption. Earlier reports suggest that metal chalcogenides are unstable leading to photoanodic corrosion,[55] which could in principle lead to stability loss of the used catalyst. However, prepared composites were found to have good photostability, which confirms their promise in photocatalyst applications. Table 1 gives an overall comparison of the present catalyst with the other reported graphene based photocatalyst operated under different experimental parameters. A comparison table is given with the literature reports to show the superiority of the CuS/rGO-x catalyst.

Kinetics Study

Two kinetic models viz. pseudo first and pseudo second order have been used to analyze the methylene blue photocatalytic decomposition using CuS/rGO nanocomposites.[67] Experimental results were fit and analyzed by the above two models. The below equation was utilized to calculate the amount of MB adsorbed.

$$q_t = \frac{(C_o - C_t)\,V}{m} \quad (3)$$

where, the initial and final concentrations of the methylene blue dye solution are C_o and C_t in mg/L, q_t in mg/g represents the quantity of MB dye absorbed, V represents amount of dye in mL and m represents the initial weight of the CuS/rGO taken in mg.

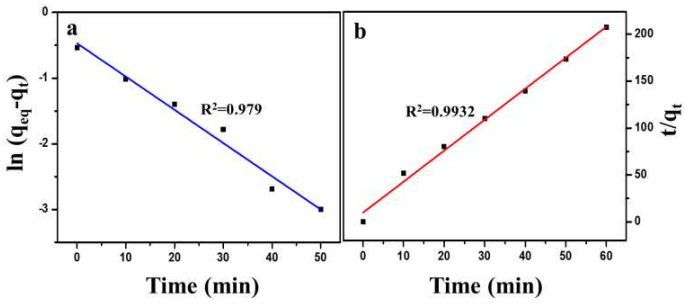

Fig. 11 Adsorption kinetic study of MB with CuS/rGO-x nanocomposites for (a) pseudo- first-order model and (b) pseudo second-order model

The equation for order model is given as follows:

$$\ln(q_e - q_t) = \ln q_e - k_1 t \quad (4)$$

where q_e and q_t represents the capacity of adsorption at equilibrium and time t; k_1 is the pseudo first order rate constant. A graph plotted between log (q_e-q_t) and time is shown in Fig. 11a. This equation was not a good fit since less correlation coefficient was obtained CR (0.979). The equation for pseudo second order model as follows:

$$\frac{t}{q_t} = \left(\frac{t}{k_2 q e_2}\right) + \frac{t}{q_e} \quad (5)$$

where q_t represents the quantity of dye absorbed in mg/g at time t; k_2 is pseudo second order rate constant. A graph plotted between t/q_t and time is linear with a high correlation coefficient, 0.9932 and hence MB degradation using CuS/rGO-x catalyst follows pseudo second order kinetics.

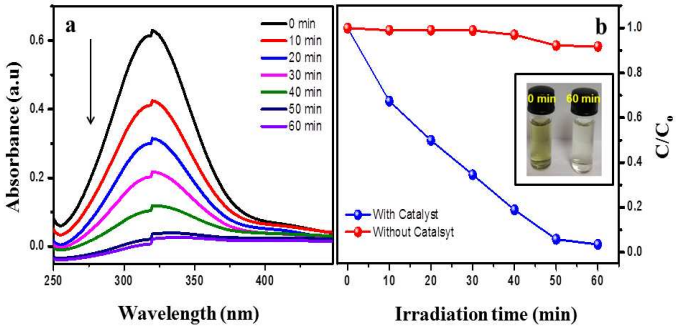

Fig. 12. Photodegradation of 4-nitrophenol (a) C/Co plot vs irradiation time under visible light irradiation for CuS/rGO-x nanocomposites (b) (inset shows before and after degradation)

Organic contaminants and textiles effluents pose major threat to human beings, fauna and flora. In this necessity, the catalytic property of CuS/rGO-x nanocomposite was further tested towards the degradation of organic contaminant and textile effluents collected from two different industrial sites situated in the Thirupur textile industries, Tamil Nadu, India.

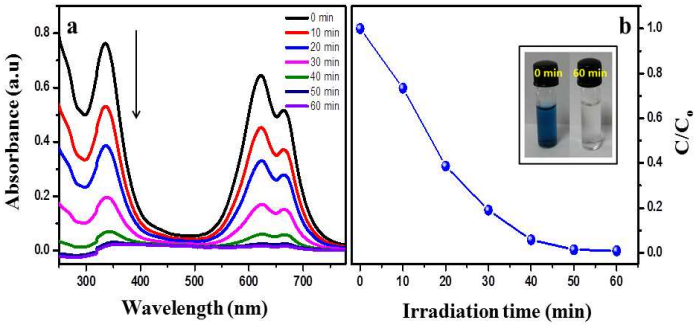

Fig. 13. Photodegradation of industrial effluent from site A (a) C/Co plot vs irradiation time under visible light irradiation for CuS/rGO-x nanocomposites (b) (inset shows before and after degradation)

The textile effluent samples were collected before the effluent treatment from the industries. The photodegradation of 4-nitrophenol and textile effluent was tested under visible light irradiation. Fig. 12 shows the photodegradation of 4-nitrophenol and Fig. 13 & 14 shows the degradation graph of textile effluents. All the experiments were carried out in visible light under similar conditions.

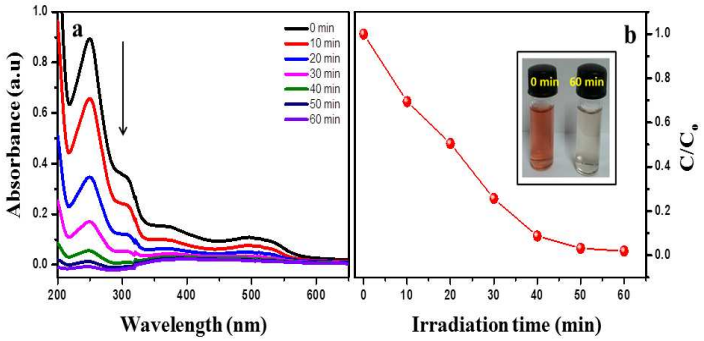

Fig. 14. Photodegradation of industrial effluent from site B (a) C/Co plot vs irradiation time under visible light irradiation for CuS/rGO-x nanocomposites (b) (inset shows before and after degradation)

The obtained results shows that CuS/rGO-x nanocomposite act as a very good photocatalyst for the pollutant removal, upto 99% of contaminant was removed after 60 min visible light irradiation.

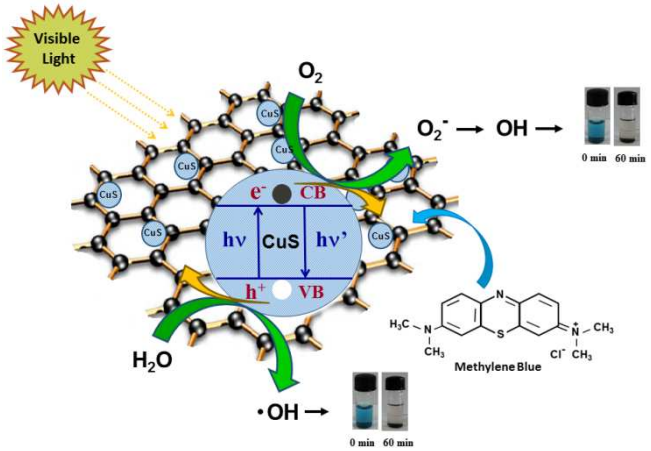

Scheme 2. Mechanism of Photocatalysis

It is well known that photocatalysis occurs through the adsorption/desorption phenomena occurring on the surface of the catalyst. The mechanism of photocatalysis is given in Scheme 2. As a narrow band gap semiconducting material, CuS absorbs more photons than materials with a wider band gap, which results in enhanced photocatalysis in visible light. The important factors governing this photocatalytic process are the effective adsorption of the MB dye molecules onto the CuS surface and the efficient separation of photogenerated e^-/h^+ pairs. In this system, the CuS/rGO-x photocatalyst degrades the dye and the dye molecules adsorb on its surface. The adsorption of MB onto the CuS/rGO-x catalyst is due to the primary

atomic force field and the pi-pi interactions of the catalyst with the dye. Adsorption creates a rich dye environment on the catalyst surface there by enhancing the reaction rate. The presence of rGO is likely to improve photogenerated e^-/h^+ pair separation and further promote photogenerated charge transfer. The possible electron movements from the conduction band of CuS to GO are described by the following equations:[68]

$$CuS + h\upsilon \rightarrow CuS(e+h) \quad (6)$$

$$CuS(e) + O_2 + GO \rightarrow CuS + O_2 + GO(e) \quad (7)$$

$$CuS(h) + OH^- \rightarrow CuS + {}^{\bullet}OH \quad (8)$$

$$CuS(h) + {}^{\bullet}OH + MB \rightarrow Degradation\ products \quad (9)$$

When the CuS/rGO catalyst absorbs light in the visible region, an e^-/h^+ pair will be generated; upon light absorption, electron excited from valance band and energy in excess is utilized to transfer it to the conduction band resulting in the generation of electron/hole pair. This in-turn helps in regulating the photocatalytic process. Photo-excitation of the electron from CuS to the rGO sheets assists charge separation by generating more •OH radicals for the degradation of dye molecules.[18] These excited electrons can transfer the energy to graphene sheets and get energy from excitation levels of graphene sheets. Holes from the valence band breaks the H_2O and leads to the formation of •OH radicals, hence in-turn degrade the dye molecules. The CB e^- reacts with O_2 molecule to form a super oxide ion ($\bullet O_2^-$), which can also react with further dye molecules. Thus overall the active species generated enhances the photocatalytic process.[69] Thus with visible light source using CuS/rGO-x catalyst, large amounts $\bullet O_2^-$ and •OH are generated which enhances the degradation of the methylene blue dye.[70] Also, the addition of H_2O_2 to CuS in dye solution resulted in an increase in the degradation ratio. The H_2O_2 acted as electron acceptors to decrease the electron/hole recombination and hence increased the concentration of •OH radicals.[71] The photogenerated electron of CuS are captured and transferred by rGO, thereby reducing the recombination rate of photoelectron-hole pairs. Overall the photocatalytic efficacy of the prepared composite is due to the cumulative contribution from rGO and CuS. The rGO provides two-dimensional support and sufficient surface area for the deposition of the CuS nanoparticles. The adsorption ability of the composites is enhanced by the presence of the rGO sheets. The synergistic effect between graphene and CuS nanoparticles in the CuS/rGO-x nanocomposite allows graphene to capture or trap the photo-induced electrons from the conduction band of the CuS through the extended π-conjugation carbon network, and consequently restrict the flash recombination of electron–hole pair.[72] Therefore, CuS/rGO-x is expected to show higher photocatalytic activity when compared to the other nanocomposites. Consequently, increasing the amount of rGO content in the rGO/CuS nanocomposite introduces new charge recombination centres for photoinduced charge separation, and as a consequence this decreases the photocatalytic efficiency.

Conclusion

This study investigated the synthesis with a simple hydrothermal method of CuS/rGO nanocomposites with various loadings of rGO and characterized the resulting materials. The XRD patterns of the nanocomposites revealed that they consist of pure hexagonal phase with high crystallinity. The prepared composites were tested in methylene blue dye degradation; the maximum degradation over 60 min was that of the CuS/rGO-x nanocomposite, 99%. It was also found that the decomposition of MB on the CuS/rGO composites follows pseudo second order kinetics. The enhanced photocatalysis and good recyclability of the catalyst mean that it is a useful and potent catalyst for photocatalytic applications.

Conflict of Interest

The authors declare no conflict of interest.

Notes

[a]*Centre for Nanotechnology Research, VIT University, Vellore 632014, India. E-mail: anirmalagladys@gmail.com; anirmalagrace@vit.ac.in;*
[b]*Thin Film Magnetism Group, Department of Physics, University of Cambridge, Cambridge CB3 0HE, United Kingdom.*
[c]*Climate Change Technology Research Division, Korea Institute of Energy Research, Yuseong-gu, Daejeon. 305-343, South Korea.*

* To whom correspondence should be addressed:
E-mail: anirmalagrace@vit.ac.in, anirmalagladys@gmail.com, jeongsk@kier.re.kr;
Tel.: (+91) 416 2202412, (+82) 42 860 3367, Fax: (+91) 416 2243092, (+82) 42-860-3134.

References

1 A.O. Ibhadon and P. Fitzpatrick, *Catalysts*, 2013, **3**, 189-218.
2 J.P. Guin, D. Naik, Y.K. Bhardwaj and L. Varshney, RSC Adv., (In press), 2014.
3 K. Hashimoto, H. Irie and A. Fujishima, Jpn. *J. Appl. Phys.,* 2005, **44**, 8269-8285.
4 W. Jia, B. Jia, F. Qu and X. Wu, *Dalton Trans.*, 2013, **42**, 14178-14187.
5 J. Kundu and D. Pradhan, *ACS Appl. Mater. Interfaces*, 2014, **6**, 1823-1834.
6 X. Jiang, Y. Xie, J. Lu, W. He, L. Zhu and Y. Qian, *J. Mater. Chem*, 2000, **10**, 2193-2196.
7 L. Quan, W. Li, L.Zhu, X. Chang and H. Liu, RSC Adv., 2014, **4**, 32214-32220.
8 M. Basu, A.K. Sinha, M. Pradhan, S. Sarkar, Y. Nehishi, Govind and T. Pal, *Environ. Sci. Technol*, 2010, **44**, 6313-6318.
9 C. Xing, L. Zhang, X. Lu, X. Bian, B. W. Sun and C. Wang, *Dalton Trans.*, 2013, **42**, 14006-14013.
10 M. Saranya, C. Santhosh, R. Ramachandran, P. Kollu, P. Saravanan, M. Vinoba, S.K. Jeong and A.N. Grace, *Powder Technol*, 2014, **252**, 25-32.
11 P. Roy and S.K. Srivastava, *Cryst Growth Des.*, 2006, **6**, 1921-1926.
12 T. Zhao, Y. Zhao, L. Jiang, *Phil. Trans. R. Soc. A.*, 2013, **371**.
13 Z. Cheng, S. Wang, Q. Wang and B. Geng, *Cryst Eng Comm*, 2010, **12**, 144-149.

14 X. Meng, G. Tian, Y. Chen, R. Zhai, J. Zhou, Y. Shi, X. Cao, W. Zhou and H. Fu, *Cryst Eng Comm*, 2013, **15**, 5144-5149.
15 B. Wang, M. K. H. Leung, X. Y. Lu and S. Y. Chen, *Appl. Energy*, 2013, **112**, 1190-1197.
16 J. Yu, J. Xiong, B. Cheng and S. Liu, *Appl. Catal. B*, 2005, **60**, 211-221.
17 R. Ramachandran, M. Saranya, C. Santhosh, V. Velmurugan, B.P.C. Raghupathy, S.K. Joeng and A.N. Grace, RSC Adv., 2014, **4**, 21151-21162.
18 S. Stankovich, D.A. Dikin, G.H.B. Dommett, K.M. Kohlhaas, E.J.Zimney, E.A. Stach, R.D. Piner, S.T. Nguyen and R.S. Ruoff, *Nature*, 2006, **442**, 282-286.
19 X. Huang, X. Qi, F. Boey and H. Zhang, *Chem. Soc. Rev.*, 2012, **41**, 666-686.
20 S.J. Park, K.S. Lee, G. Bozoklu, W.W. Cai, S.T. Nguyen and R.S. Ruoff, *ACS Nano*, 2008, **2**, 572- 578.
21 A.N. Grace, R. Ramachandran, M. Vinoba , S.Y. Choi, D.H. Chu,Y. Yoon, S.C. Nam and S.K. Jeong, Electroanalysis, 2014, **26**, 199-208.
22 S. Giri, D. Ghosh and C. K. Das, *Dalton Trans.*, 2013, **42**, 14361-14364.
23 J. Zhang, H. Yang, G. Shen, P. Cheng, J. Zhang and S. Guo, *Chem.Commun*, 2010, **46**, 1112-1114.
24 Y. Liu, D. Yu, C. Zeng, Z. Miao and L. Dai, *Langmuir*, 2010, **26**, 6158-6160.
25 X. Sun, Z. Liu, K. Welsher, J.T. Robinson, A. Goodwin, S. Zaric and H. Dai, *Nano. Res.*, 2008, **1**, 203-212
26 H. Chang and H. Wu, *Energy, Environ. Sci.*, 2013, **6**, 3483-3507.
27 Y. Su and I. Zhitomirsky, *Colloids Surf., A.*, 2013, **436**, 97-103.
28 Y. Ding, Y. Jiang, F. Xu, J. Yin. H. Ren, Q. Zhou, Z. Long and P. Zhang, *Electrochem Commun*, 2012, **12**, 10-13.
29 S. Song, W. Gao, X. Wang, X. Li, D. Liu, Y. Xing and H. Zhang, *Dalton Trans*., 2012, **41**, 10472-10476.
30 S. Anandhavelu and S. Thambidurai, *Electrochim Acta*, 2013, **90**, 194-202.
31 Z. Gao, W. Yang, J. Wang, H. Yan, Y. Yao, J. Ma, B. Wang, M. Zhang and L. Liu, *Electrochim Acta*, 2013, **91**, 185-194.
32 L. Zhang, Z. Wang, L. Wang, Y. Xing, Y and Zhang, *Mater Lett.*, 2013, **108**, 9-12.
33 X. Liu, L. Pan, Q. Zhao, T. Lv, G. Zhu, T. Chen, T. Lu, Z. Sun and C. Sun, *Chem. Eng. J*., 2012, **83**, 238-243.
34 M. Saranya, G. Srishti, S. Iksha, R. Ramachandran, C. Santhosh, C. Harish, T. Vanchinathan, M. Bhanu and A.N. Grace, *Nanosci. Nanotechnol. Lett*, 2013, **5**, 349-354.
35 X.H. Guan, P. Qu, X. Guan and G. S. Wang, RSC Adv., 2014, **4**, 15579-15585..
36 X. Wang, H. Li, Y. Liu, W. Zhao, W. Zhao, C. Liang, H. Huang, D. Mo, Z. Liu, X. Yu, Y. Deng and H. Shen, *Appl. Energy*, 2012, **99**, 198-205.
37 W. S. Hummers and R. E. Offeman, *J Am Chem Soc*, 1958, **80**, 1339-1339.
38 Z.Gao, N. Liu, D. Wu, W. Tao, F. Xu and K. Jiang, *Appl. Surf. Sci.*, 2012, **258**, 2473-2478.
39 K. Chang and W.X. Chen, *ACS Nano*, 2011, **5**, 4720−4728.
40 H. C. Zeng, *Curr. Nano Sci*, 2007, **3**, 177-181.
41 Q. Lu, F. Gao and D. Zhao, *Nano Lett.*, 2002, **2**, 725-728.
42 H. Qi, J. Huang, L. Cao, J. Wu and J. Li, *Ceram. Int.*, 2012, **38**, 6659-6664.
43 C. Yang, H. Fan, Y. Xi, J. Chen and Z. Li, *Appl. Surf. Sci*., 2007, **254**, 2685-2689.
44 K. Mageshwari, S.S. Mali, T. Hemalatha, R. Sathyamoorthy and P.S. Patil, *Prog. Solid State Chem*., 2011, **39**,108-113.
45 S.K. Maji, N. Mukherjee, A.K. Dutta, D.N. Srivastava, P. Paul and B. Karmakar, *Mater. Chem. Phys.*, 2011, **130**, 392-397.
46 J. Liqiang, Q. Yichun, W. Baiqi, L. Shundan, J. Baojiang, Y. Libin, F. Wei, F. Honggang and S. Jiazhong, *Sol. Energy Mater. Sol. Cells*, 2006, **90**, 1773-1787.
47 J. Zhou, F. Zhao, X. Wang, Z. Li, Y. Zhang and L. Yang, *J. Lumin.*, 2006, **237**, 237-241.
48 L.Z. Pei, J.F. Wang, X.X. Tao, S.B. Wang, Y.P. Dong, C.G. Fan and Q.F. Zhang, *Mater.Charact.*, 2011, **9**, 354-359.
49 Y. Fu, H. Chen, X. Sun and X. Wang, *Appl. Catal. B,* 2012, **111-112**, 280-287.
50 J. Zhang, J. Yu, Y. Zhang, Q. Li and J.R. Gong, *Nano Lett*., 2011, **7**, 4774-4779.
51 G. Nie, Z. Li, X. Lu, J. Lei, C. Zhang and C. Wang, *Appl. Surf. Sci*., 2013, **284**, 595-600.
52 J. Yu, T. Ma and S. Liu, *Phys. Chem. Chem. Phys*., 2013, **13**, 3491-3501.
53 Q. Li, B. Guo, J. Yu, J. Ran, B. Zhang, H. Yan and J.R. Gong, J. Am. Ceram, Soc., 2011, **133**, 10878-10884
54 N.A. Zubir, C. Yacoul, J. Motuzas, X. Zhang, J.C. Diniz da Costa, Sci. Rep., 2014, **4**, 4594.
55 D.S. Bhastkhande, V.G. Pangarkar and A.C.M. Beenackers, *J. Chem. Technol. Biot*., 2002, **77**, 102−116.
56 D. Zhao, G. Sheng, C. Chen and X. Wang, Appl. Catal., B: Environ., 2012, **111**-**112**, 303-308.
57 J. Li, S.I. Zhou, G.B. Hong and C.T. Chang, Chem. Eng. J., 2013, **219**, 486–491
58 Z. Gao, J. Liu, F. Xu, D. Wu, Z. Wu and K. Jiang, Solid State Sci., 2012, **14**, 276–280.
59 N.R. Khalid, E. Ahmed, Z. Hong and M. Ahmad, Appl. Surf. Sci., 2012, **263**, 254-259.
60 A.A. Ismail, R.A. Geioushy, H. Bouzid, S.A. Al-Sayari, A. Al-Hajry and D.W. Bahnemann, Appl. Catal., B: Environ., 2013, **129,** 62-70.
61 X. Zhou, T. Shi, J. Wu and H. Zhou, Appl. Surf. Sci., 2013, **287**, 359-368.
62 H.R. Pant, C.H. Park, P. Pokharel, L.D. Tijing, D.S. Lee and C.S. Kim, Powder Technol., 2013, **235**, 853-858.
63 H. Sun, S. Liu, S. Liu and S. Wang, Appl. Catal., B: Environ., 2014, **146**, 162-168.
64 P. Dong, Y. Wang, B. Cao, S. Xin, L. Guo and J. Zhang, F. Li, Appl. Catal., B: Environ., 2013, **132**-**133**, 45-53.
65 Y. Zhang, J. Tian, H. Li, L. Wang, X. Qin, A.M. Asiri, A.O. Al-Youbi and X. Sun, Langmuir, 2012, **28**, 12893-12900.
66 X. Wang, H. Tian, Y. Yang, H. Wang, S. Wang, W. Zheng, Y. Liu and J. Alloys Compd., 2012, **524**, 5-12.
67 M. Zhou, X. Gao, Y. Hu, J. Chen and X. Hu, *Appl. Catal. B*, 2013, **138-139**, 1-8.
68 A.A. Ismail, R.A. Geioushy, H. Bouzid, S.A. Al-Sayari, A. Al-Hajry and D.W. Bahnemann, *Appl. Catal. B*, 2013, **129**, 62-70.
69 H. Zhang, X.F. Fan, X. Quan, S. Chen and H.T. Zu, *Environ. Sci. Technol*., 2011, **45**, 5731-5736.
70 I.A. Salem and M.S. El-Maazawi, *Chemosphere*, 2000, **41**, 1173-1180.
71 J. Yao and C. Wang, Int. J. Photoenergy, 2010, Article ID 643182.
72 K. Ullah, S. Yu, Z. Lei, K.Y. Cho and W.C. Oh, Catal. Sci. Technol., 2014 (In press).

